Comparison of colloidal silica involved fouling behavior in three membrane distillation configurations using PTFE membrane

Comparison of colloidal silica involved fouling behavior in three membrane distillation configurations using PTFE membrane

Wenli Qin[a,c]; Zongli Xie[a,*], Derrick Ng[a], Ying Ye[c], Xiaosheng Ji[c], Stephen Gray[b], Jianhua Zhang [b,*]

a. CSIRO Manufacturing, Private bag 10, Clayton South MDC, Vic. 3169, Australia

b. Institute for Sustainability and Innovation, Victoria University P.O. Box 14428, Melbourne, Vic 8001, Australia

c. Institute of Marine Geology and Resource, Ocean College, Zhejiang University, Zhoushan, Zhejiang 316021, China

Abstract:

Colloidal silica involved fouling behaviors in direct contact membrane distillation (DCMD), vacuum membrane distillation (VMD) and sweeping gas membrane distillation (SGMD) were studied. Three foulants were used in the experiments, including colloidal silica as representative of particulate foulants, calcium bicarbonate as dissolved inorganic foulant, and NOM (humic acid + alginate + BSA) as the dissolved organic foulant. The three types of fouants were combined to produce four different feed waters: silica alone; silica + calcium bicarbonate; silica + NOM; and silica + calcium bicarbonate + NOM. With 25% feed recovery, it was found that VMD showed the worst performance for most of the foulant combinations due to turbulence

dead zones caused by the membrane deformation that increased foulant deposition. For the silica + calcium bicarbonate + NOM feed DCMD had the greatest fouling rate, although DCMD also had the highest flux of all configurations. SGMD showed the best fouling resistance of all configurations, although it was inclined to calcium carbonate fouling because carbon dioxide was removed in the permeate leading to calcium carbonate precipitation and could be alleviated by using air as sweeping gas. For feeds containing high-concentration calcium bicarbonate or carbonate foulants, VMD should be avoided to lower the formation of carbonate precipitants on the membrane surface if scale inhibitors are not used.

Key words: Membrane distillation; membrane fouling; colloidal silica; MD configuration

1. Introduction:

Membrane distillation (MD) is a hybrid of thermal distillation and membrane separation described in technical literature since 1967 (Banat et al. 2002, Lawson and Lloyd 1997, Lei et al. 2005, Weyl 1967). Although a membrane is involved in MD, the driving force is quite different from other membrane processes, being the vapour pressure difference across the membrane which drives mass transfer through a membrane (Lawson and Lloyd 1997, Schneider and van Gassel 1984), rather than an applied pressure difference, a concentration gradient or an electrical potential gradient.

MD has 100% theoretical rejection to non-volatile components and is proposed to

be utilised with low grade heat sources of 40-80°C (Zhang et al. 2010b). Since the driving force of MD is a partial vapour pressure difference across a membrane commonly triggered by a temperature difference, its flux is not likely sensitive to feed salinity in practical water treatment. Therefore, MD can be combined with conventional reverse osmosis (RO) processes to increase water recovery and minimise high concentration brine discharge. Therefore, MD can combine with conventional reverse osmosis (RO) processes to minimise high concentration brine discharge. However, to achieve high RO recovery in zero liquid discharge processes, the RO concentrate will be nearly saturated or saturated by some low solubility inorganic and organic salts, such as humic acid, calcium bicarbonate, and colloidal silica, which are major foulants for membrane process. Although MD shows much better fouling resistance than RO, it still suffers from fouling problems (Gryta 2008, Warsinger et al. 2015). Membrane fouling in MD will reduce productivity, deteriorate permeate quality, increase energy consumption and treatment cost, shorten membrane life span , and even cause membrane wetting (Qin et al. 2017).

PTFE membrane has desirable characteristics for use in membrane distillation. The PTFE has high hydrophobicity with surface energy of 9.1 kN/m (Mulder 1996). Its thermal conductivity is as low as 0.22-0.45 $Wm^{-1}K^{-1}$ and has excellent chemical stability at the operating temperatures of membrane distillation (Alklaibi and Lior 2005). Furthermore, the porosity of PTFE membrane can be as high as 90% (Zhang et al. 2010a). However, the PTFE membrane is not as rigid as PVDF membrane and can be deformed easily under pressure which will affect its performance (Zhang et al. 2011).

In MD processes, one side of the membrane contacts the liquid feed. Depending on the permeate collection design, four MD configurations are generally recognised: DCMD, Air Gap Membrane Distillation (AGMD), VMD and SGMD (Alklaibi and Lior 2005, Zhang et al. 2013b). While these processes operate in a similar manner, they have different operating characteristics with DCMD usually resulting in higher flux but lower thermal energy efficiency, and AGMD higher thermal energy efficiency but lower flux (Lei et al. 2005).

Previous MD fouling studies have generally considered only one particular MD configuration (Qin et al. 2017, Wang et al. 2016a, Wang et al. 2016b), and there has been little research focused on comparison of fouling behaviour of MD configurations, especially for feeds containing colloidal silica. In this study, the performance of the DCMD, SGMD and VMD were studied using synthetic feeds with different types of foulant combination. Furthermore, the influence of PTFE membrane compression on fouling behaviours is also discussed. While AGMD is more commonly considered than SGMD, we have previously found that the gap distance in AGMD is very hard to control experimentally when flexible PTFE membrane is used. While other researchers have not reported such experimental issues, we have been concerned with the membrane directly contacting the cooling plate and affecting the fouling behaviour. Furthermore, this configuration is very complex for fabrication, and permeate can build up in the gap leading to operation as permeate gap membrane distillation. Therefore, flowing air was used to keep the channel clear of liquid.

In this study, we focused on the influence of permeate collection methods in

different configurations on the feed side fouling, which was rarely researched but important for MD commercialisation.

2. Materials and Method:

2.1 Materials

A hydrophobic, microporous membrane from Changqi Ltd. (Ningbo, China) was used in the MD experiment. The membrane consisted of a thin polytetrafluoroethylene (PTFE) active layer (thickness 30 μm) on top of a polypropylene (PP) support layer with a total membrane thickness of 120 μm. The nominal pore size and porosity of the PTFE active layer were 0.5 μm and 90 %, respectively.

Ludox HS-40 silica colloids (particle size = 12 nm) from Sigma-Aldrich were used to represent a colloidal/particulate foulant; humic acid (Sigma-Aldrich), alginate (Sigma-Aldrich) and bovine serum albumin (BSA, Sigma-Aldrich)) were used to represent natural organic matter; calcium carbonate was used as the dissolved inorganic foulant synthesized by calcium chloride and sodium bicarbonate. A stock solution (5 g L^{-1}) with each organic foulant was prepared by dissolving each organic foulant into Milli-Q water and stored in a sterilized amber glass bottle at 4°C. The Ludox HS-40 colloidal silica suspension (40 wt. %) was sonicated for 10 min to ensure complete dispersion before adding to the feed solution. All the feeds contained NaCl (1 mol/L) and colloidal silica (1000 mg/L), and depending on the combination, also contained $Ca(HCO_3)_2$ (648mg/L) and/or natural organic matter (NOM) that consisted of humic acid (200 mg/L), alginate (200 mg/L), and BSA (200 mg/L).

2.2 Membrane testing

Figure 1 shows a schematic of the laboratory MD system which consisted of a flat sheet membrane module made from acrylic blocks, a feed tank, a permeate tank, a circulating pump and/or a vacuum pump. The membrane was placed in the middle of the module with an effective membrane area of 65 cm^2 (membrane dimension 5 cm ×13 cm). Spacers (thickness = 0.7 mm, filament diameter = 0.35 mm, porosity = 0.87) were placed on both sides of the membrane to enhance the turbulence of the streams and guide the flow in the membrane module. The channel depths were 1 mm where the spacers were placed. The temperature of the feed solution was maintained by a water bath (DF-101S, Yuhua Instruments). The initial feed volume of different MD configurations was kept constant at 2 litre. In DCMD mode (Figure 1a), the stream velocities on both sides of the membrane were kept equal at 0.56 m/s (flow rate = 500 mL/min) and controlled by two Masterflex peristaltic pumps. An ice water cooler was used to cool the permeate stream and the temperature was maintained at 10°C for all experiments under the stable conditions. The temperatures at the inlets and outlets of both the feed and permeate streams were monitored using K-type thermocouples and the weight gain of the permeate tank on the permeate side was continuously recorded every 5 seconds using an electronic balance (± 0.1 g accuracy, model GF-6000, A&D Instruments) connected to a data logger. The water flux was determined via the weight gain of the permeate reservoir per unit area over time (5 min) and is expressed as $L/m^2 \cdot h$. The run time was about 6 h.

For SGMD (Figure 1b) and VMD systems (Figure 1c), the weight loss of the feed tank on the feed side was continuously recorded every 5 seconds using an electronic balance connected to a data logger. In SGMD system, nitrogen (N_2) was used to strip the permeate from the feed and the flowrate was maintained at 7 L/min (2.33 m/s) and monitored by a flowmeter. The run time was about 20 h. In the VMD system, a vacuum pump was utilized to produce vacuum pressure of 1.33 kPa (10 torr) and the permeate was condensed by chilled water at 5ºC in a container prior to the vacuum pump. The run time was about 10 h. On the feed sides of SGMD and VMD, the inlet temperature and flow velocity were maintained to be the same. The water flux was determined via the weight gain or loss of permeate (for DCMD) or weight loss of feed (for SGMD and VMD) reservoir per unit area over time and is expressed in the units of $L/m^2 \cdot h$. The feed tank was covered by preservative film to prevent losing water by evaporation during the test.

MD fouling experiments were conducted for DCMD, SGMD and VMD configurations. A new membrane specimen was used for each experiment. Every test was repeated at least for three times, and the results presented in this paper were the average values of the three repeats. Although the initial flux variation for each repeat was about ±5% due to the difference among the new membrane specimens, the flux decline trends were similar between the repeats. In addition, all the experiments were purposely terminated at the same water recovery rate of 25%, so the fouled membrane at the end of the experiment can be compared on the same basis.

149 Conductivity of the permeate stream was measured by a conductivity meter (CON
150 110, Oakton Instruments) every 30 minutes for DCMD, and every 120 minutes for
151 SGMD and VMD. After each fouling test, the membrane was removed from the
152 membrane cell and was kept in a desiccator for subsequent characterisation.

153 For each experiment, the minimum recovery calculated by Equation (1) was 25%.

154 $$Rec = (1 - \frac{m_t}{m_0}) \times 100\% \quad (1)$$

155 where *Rec* is the feed recovery and m_0 and m_t are the initial feed mass and mass of feed
156 at time *t* respectively.

157 The salt rejection was calculated by Equation (2).

158 $$Rej = (1 - \frac{C_{permeat}}{C_{feed}}) \times 100\% \quad (2)$$

159 where *Rej* is the salt rejection, $C_{permeate}$ and C_{feed} are the conductivities of the feed and
160 permeate, respectively.

161 For spacer filled flow channels, the local Reynolds number can be computed by
162 (Geankoplis 2003, Phattaranawik et al. 2001, Zhang et al. 2012),

163 $$Re = \frac{\rho d_h v}{\mu} \quad (3)$$

164 Here, ρ is the water density, v is the linear velocity of the feed, μ is the water
165 viscosity and d_h is the hydraulic diameter in a spacer filled channel and is calculated by

166 $$d_h = \frac{4.0 \varepsilon_s d_f h_s}{2 d_f + 4(1 - \varepsilon_s) h_s} \quad (4)$$

Here, ε_s is the spacer porosity, d_f is the spacer filament diameter, and h_s is the spacer thickness.

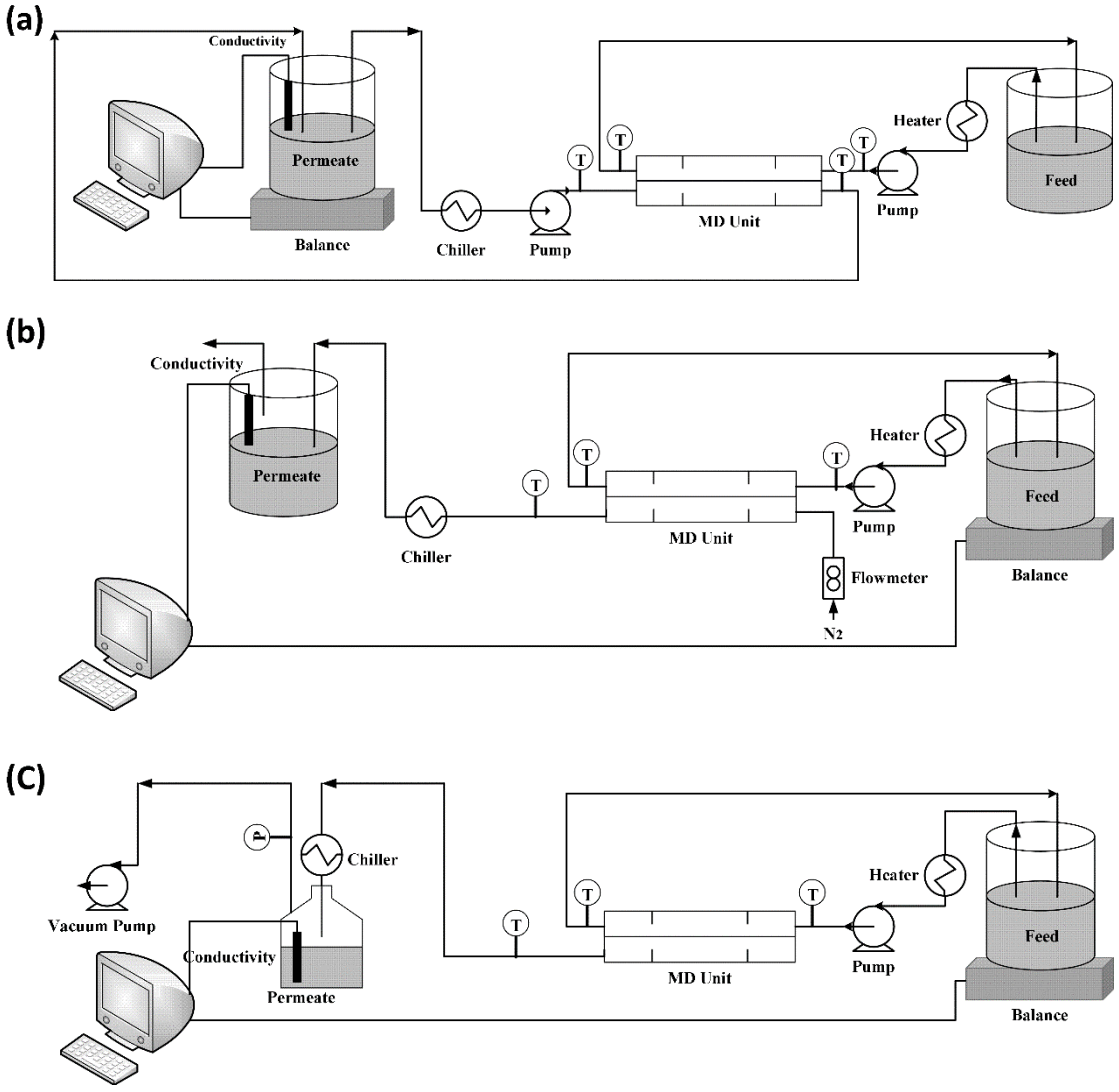

Figure 1 MD set up in the lab: (a) DCMD, (b) SGMD, (c) VMD.

2.3 Analytical methods

The morphology of the fouling layer deposited onto the membrane surface was examined by a scanning electron microscope (SEM, Zeiss Merlin FESEM). Both membrane surface and cross sectional images were taken. Distribution of fluorine (F),

carbon (C), calcium (Ca), sodium (Na), and silica in the fouled membrane cross section was mapped by energy-dispersive X-ray spectroscopy (EDS, Zeiss Merlin FESEM).

3. Results and discussions:

3.1 DCMD, VMD and SGMD fouling tests

3.1.1 Performance of different configuration

Based on Figure 2 and Table 1, the same foulant combinations had quite different influences on the flux decline magnitudes of the different MD configurations. With 25% feed recovery, the silica only feed had very little influence on DCMD (2.5% decline) and SGMD (1.7% decline) fluxes, but caused about 20.4% flux decline of VMD.

Silica+Ca combination showed little influence on the DCMD flux when the recovery was less than 23%, and led to about 8.9% flux decline with 25% recovery. However, for SGMD and VMD, Silica+Ca combination showed a stronger influence on flux than that of DCMD, and caused 11.7% and 25.2% flux decline respectively for 25% recovery.

Si+NOM combination also had very little influence on SGMD flux (1.2% flux decline), but caused about 20.6% flux decline of VMD and 16.7% flux decline of DCMD.

At 25% recovery, it can be seen in Table 1 that the Si+Ca+NOM combinations showed the worst fouling to all configurations. DCMD showed the least resistance to this foulant combination and had a flux decline about 51.4%. SGMD and VMD had flux decline 14.4% and 30.4% respectively.

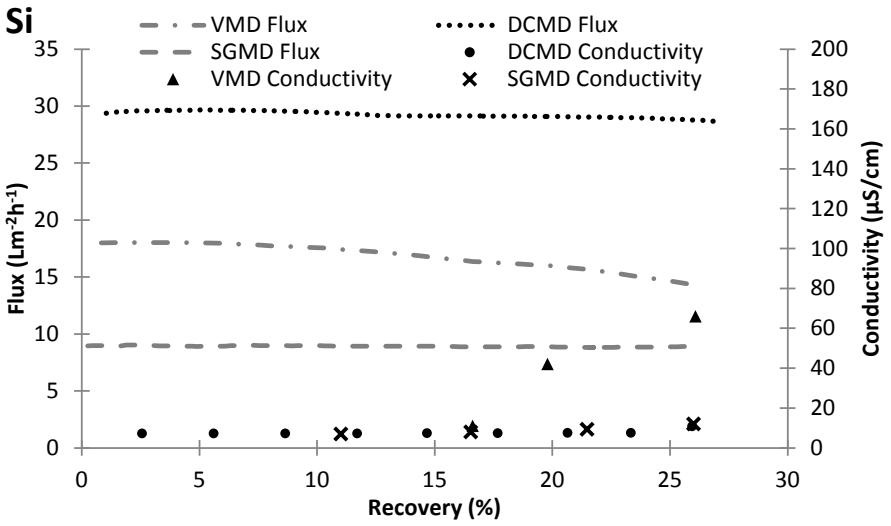

198

199 (a) Silica

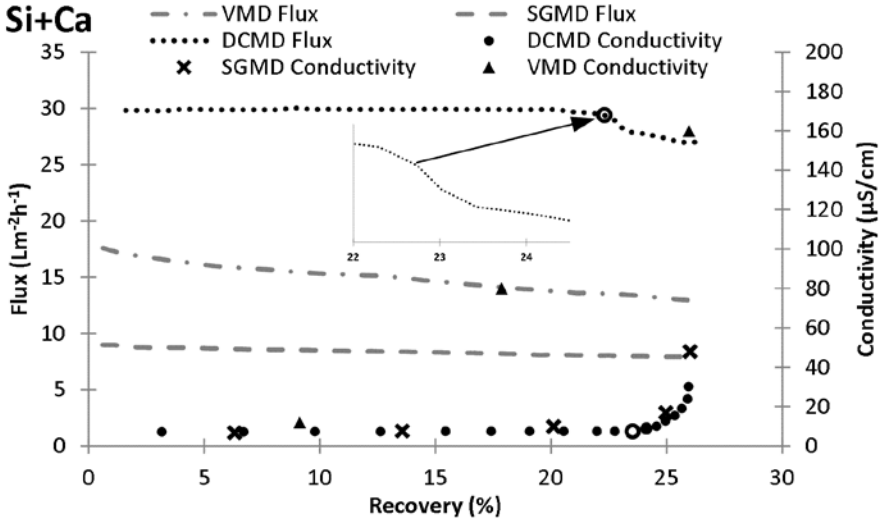

200

201 (b) Silica and $Ca(HCO_3)_2$

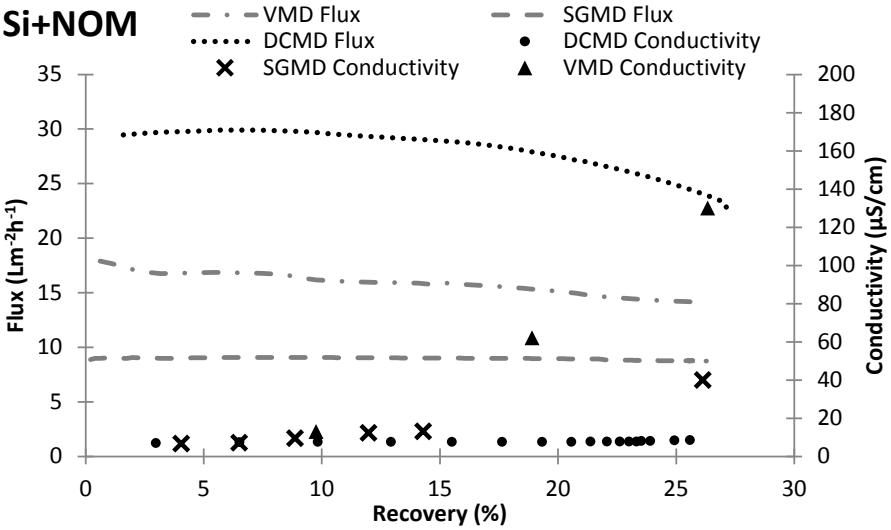

202

(c) Silica and NOM

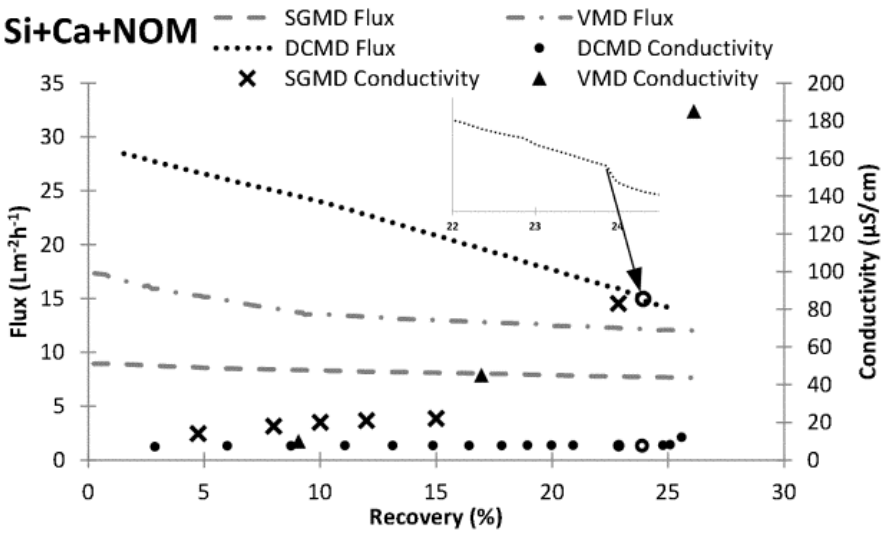

(d) Silica, $Ca(HCO_3)_2$ and NOM

Figure 2. Water flux and permeate conductivity as a function of water recovery during membrane distillation fouling in different configurations (DCMD: feed inlet temperatures = 40ºC and permeate inlet temperature = 10ºC, feed and permeate velocities were 0.56 m/s in countercurrent mode; SGMD: feed inlet temperatures = 40ºC, N_2 velocity = 2.33 m/s (7 L/min); VMD system, the vacuum pressure = 1.33 kPa).

Table 1. Percentage of flux decline at 25% recovery (experimental error ±5%)

Foulants	Flux Decline (%)		
	DCMD	SGMD	VMD
Si	2.5	1.7	20.4
Si + Ca	8.9	11.7	25.2
Si + NOM	16.7	1.2	20.6

Si + Ca+ NOM	51.4	14.1	30.4

3.1.2 Discussion of the fouling behaviors in different configurations

Table 1 shows that at 25% water recovery, DCMD showed the highest percentage flux decline (51.4%) with the Si+Ca+NOM feed, and VMD showed the highest rates of fouling for the all other foulant combinations although DCMD constantly showed the highest initial fluxes in all tests. This phenomena is not consistent with traditional fouling theory, in which high flux is prone to increase fouling issues for the same hydrodynamic conditions due to the high concentration polarisation in the boundary layer (Bacchin et al. 2006, Chen et al. 1997).

Since the feed side hydrodynamic conditions were similar in all the tests, the reason is most likely to arise from changes in membrane property for VMD configuration. PTFE material can be deformed under strain or compression (Rae and Brown 2005, Rae and Dattelbaum 2004). The PTFE membrane used in the test had porosity of approximately 90%, and was supported by scrim as shown in Figure 3(a) (Zhang et al. 2010a). Membrane compaction under high compression pressure can lead to a loss of the membrane permeability, although initially membrane permeability increase was found under low compression pressure (Lawson et al. 1995, Zhang et al. 2012). In Figure 4, schematic diagrams for PTFE membrane in different configurations are shown. It can be seen that the pressure on both sides of the membrane is balanced in DCMD and SGMD. Therefore, although PTFE is very soft material and the membrane porosity is about 90%, the membrane surface will not be deformed and pressed into the

supporting scrim. However, in VMD, the unbalanced pressure (hydraulic pressure + the vacuum pressure > 1 bar) applied only on one side of the PTFE membrane and was able to push the soft PTFE membrane into the void space of the scrim. The deformation of membrane can be observed by Figures 3(b), 3 (d), and all the following SEM images of the membrane cross section used in the VMD. Therefore, although the feed flow channel of the MD process was filled with spacer to increase turbulence (*Re* = 954) and reduce temperature polarisation and membrane fouling (Zhang et al. 2012), the deformed section in VMD formed tiny static quiescent zone or dead zones as shown in Figure 3(b) reduced the turbulence effect of the spacer and encouraged the formation of the fouling layer and increase temperature polarisation. It also can be found from Figures 3(c) and (d) that the foulant accumulated in the concaved section. The nominal driving force (vapour pressure difference) across the membrane of VMD and DCMD were all about 6 kPa respectively based on the Antoine equation (Zhang et al. 2010a). However, the VMD initial flux was only about 60% of that of DCMD, which can be explained by increased temperature polarisation and membrane compression (Lawson et al. 1995, Zhang et al. 2013a, Zhang et al. 2012).

It also can be seen in Table 1 that the foulant combinations were also key factors that determine the extent of fouling, and it is proposed that the extent of fouling can be determined by either flux or turbulence effects. For the VMD and SGMD, both low flux configurations, the Si+NOM combination showed almost the same influence on flux as the Si feed. However, the Si+NOM combination caused the second highest flux loss (16.7%) for higher flux DCMD operation at 25% recovery. Therefore, the addition of

NOM led to fouling was more flux or flux incurred concentration polarisation dependent than turbulence dependent, since NOM was solute in the feed. In contrast, silica fouling was more turbulence dependent than flux or flux incurred concentration polarisation dependent due to its particulate properties, as identified by the higher flux loss for VMD upon deformation of the membrane. The combination of the three foulants enhanced both the flux/concentration polarisation (DCMD) and turbulence (VMD) dependences of the fouling process, due to the interactions between these foulants (Kitano et al. 1969, Laqbaqbi et al. 2017, Qin et al. 2017). Furthermore, it can be seen from Table 1, the enhancement of dependence was more pronounced on flux/concentration polarisation than turbulence by comparing DCMD with VMD for combinations of three foulants.

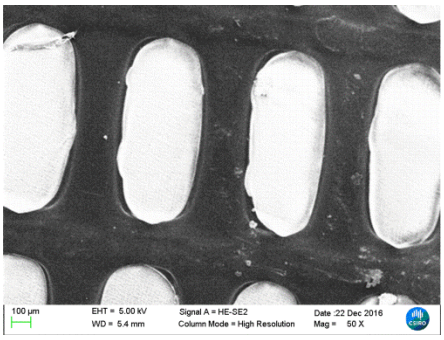

(a) Scrim

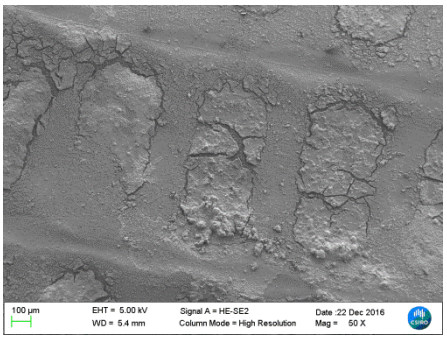

(b) Concave membrane surface following VMD operation

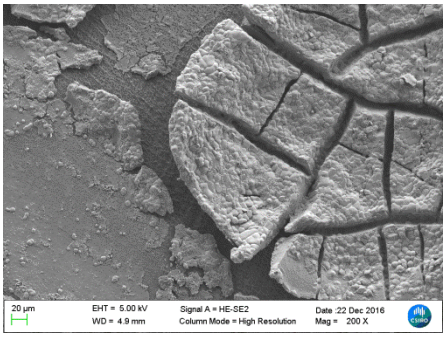

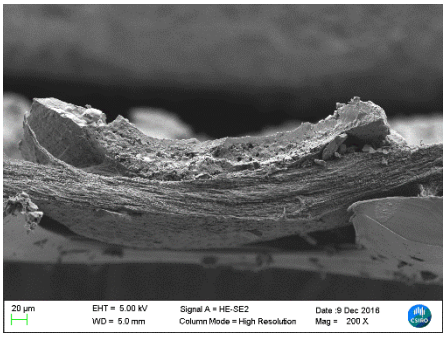

(c) Foulant in the concaved section following VMD processing

(d) Cross-section of the concaved section following VMD operation

Figure 3. Concaved sections of VMD membrane

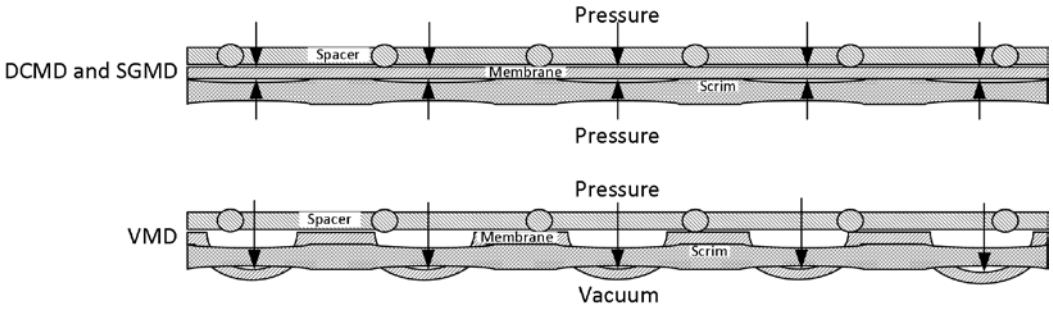

Figure 4. Schematic diagrams for PTFE membrane in different configuration

From Table 1, it is also found that calcium carbonate fouling showed less influence on DCMD flux than that of VMD and SGMD. This was mainly caused by the faster decomposition of the dissolved $Ca(HCO_3)_2$ in VMD and SGMD than that of DCMD, which eventually formed $CaCO_3$. The equilibrium of $Ca(HCO_3)_2$ vs $CaCO_3$ is shown in Eq. (3). If CO_2 in Eq. (3) is removed from the system, the equilibrium will favour the formation of $CaCO_3$. The feed during the test would reach an equilibrium under atmospheric pressure and the CO_2 concentration would be about 0.04% (Ballantyne et al. 2012). Unlike DCMD where the permeate side was also saturated with CO_2, the permeate sides of VMD and SGMD (pure nitrogen) contained negligible amount of CO_2. Therefore, the mass transfer driving force of CO_2 across the membrane was higher in VMD and SGMD than in the DCMD, and the continuous removal of CO_2 from the feed during VMD and SGMD shifted the equilibrium to the formation of $CaCO_3$ and a fouling layer on the membrane surface (Frear and Johnston 1929).

This proposition could not be well supported by the lowering pH (about 5.6) on the

permeate side, since the ionic strength was low and the values shifted with time. However, it can also be supported by conductivity variations during those tests, despite the nominal salt (NaCl) rejections calculated by Eq. (2) being higher than 99.9% for all tests. It can be seen from Figure 2a and 2c for the feed that only contained Si foulant and Si+NOM, the permeates from DCMD and SGMD only had slight conductivity change, but for VMD its permeate conductivity increased continuously due to the CO_2 depletion from the feed to the permeate side. Furthermore, the permeate conductivity for the VMD tests increased to greater than 100 μS/cm, which also suggested that wetting occurred in VMD (Enríquez et al. 2013, Gajevskiy 2015, Light et al. 1995).

$$Ca(HCO_3)_2 \Leftrightarrow CaCO_3 + H_2O + CO_2 \quad (3)$$

It is also interesting to observe that in DCMD for both calcium containing feeds, there were quick flux decline rate changes which occurred almost at the same recovery 22.5-23.5% (shown as hollow dot points in Figures 2b and 2d), accompanied with conductivity increases. This phenomenon was caused by the concentration increase of $Ca(HCO_3)_2$ due to the recovery increase, which would also cause CO_2 increase in the feed as shown in Eq. (3). When the concentration of CO_2 in the feed was higher than that in the permeate, the CO_2 would start transferring into the permeate and cause the permeate conductivity to increase. Since the CO_2 transferred from the feed to the permeate and its concentration reduced in the feed, the equilibrium as shown in Eq. (3) moved to the $CaCO_3$ formation side. Thus, the rapid flux decline was observed. Similar phenomenon can also be found in SGMD, and fast conductivity increase was observed at about 22% feed recovery, but it was not very obvious in VMD, because of the high

311 mass driving force of CO_2 and the continuous decomposition of $Ca(HCO_3)_2$.

312 *3.1.3 Surface morphology of the fouled membrane*

313 SEM and EDS images of the fouled membrane are shown in Figure 5. For the silica
314 only feed (Si), it can be observed in Figure 5(a) that both the fouling layers formed on
315 the DCMD and SGMD were more porous than that of VMD, which caused less flux
316 decline rate than that of VMD (Table 1). However, it is hard to see the difference in
317 detail from the cross section of the fouling layer in Figure 5(a), except for the VMD, in
318 which an accumulated fouling layer was observed in the deformed section of the PTFE
319 membrane.

320 Another interesting note is that, for the calcium containing silica feed (Si+Ca),
321 some spherical foulant formation was observed on the top of membrane surface in
322 DCMD, this formation is specific to DCMD as it was not present on membrane surfaces
323 in VMD and SGMD configurations. The spherical foulant (Figures 5b, 5c and 5d) was
324 calcium carbonate as suggested by others (Trushina et al. 2015, Yu et al. 2004). It can
325 be seen from Figure 2(b) that a flux decline in DCMD occurred at about 22-24%
326 recovery, which was caused by the supersaturated calcium carbonate precipitating from
327 the bulk feed and forming a calcium carbonate layer on top of the silica fouling layer.
328 However, for the VMD and SGMD processes, it is shown in Figure 2(b) that the flux
329 almost declined continuously. Therefore, the formation of calcium carbonate fouling
330 layer commenced from beginning of the tests, which was also demonstrated by EDS of
331 Figure 5(b) where the calcium was found at the bottom of the fouling layer in SGMD
332 and VMD, but only found the mostly on the top of fouling layer in DCMD.

For the NOM containing silica feed, the membrane surface and cross sectional SEM images for the different MD configurations are shown in Figure 5(c). It can be found in DCMD that a dense flat fouling layer formed on the membrane (Figure 5(c)) and the bright red carbon containing layer (EDS, Figure 5(c) in the circle) formed directly on surface of the membrane (by comparing the SEM image in the circle) under a silica dominated fouling layer due to the high flux /concentration polarisation dependence of NOM. However, the fouling layers (Figure 5(c)) for SGMD and VMD were not as smooth as that for DCMD. Furthermore, the carbon element was likely distributed on top of the silica dominated fouling layer for SGMD and distributed evenly and relative sparsely in the fouling layer of the silica dominated layer. Based on the EDS images, it can be found that NOM fouling dominated at the highest flux stage (the early stage) in DCMD prior to silica fouling, and formed at almost same time with or later than silica fouling in VMD, and only was found on the fouling layer surface in SGMD. The carbon found on the fouling layer in SGMD should not be a fouling layer and but contamination from the residual feed solution, since the NOM has an amorphous structure (Lee et al. 2004) rather than a crystal structure as shown in Figure 5(c) SGMD image. Therefore, NOM fouling formation seems more sensitive to high flux and concentration polarisation rather than that of low turbulence, since the VMD has the least turbulence in all configurations due to the membrane deformation and also the least NOM fouling.

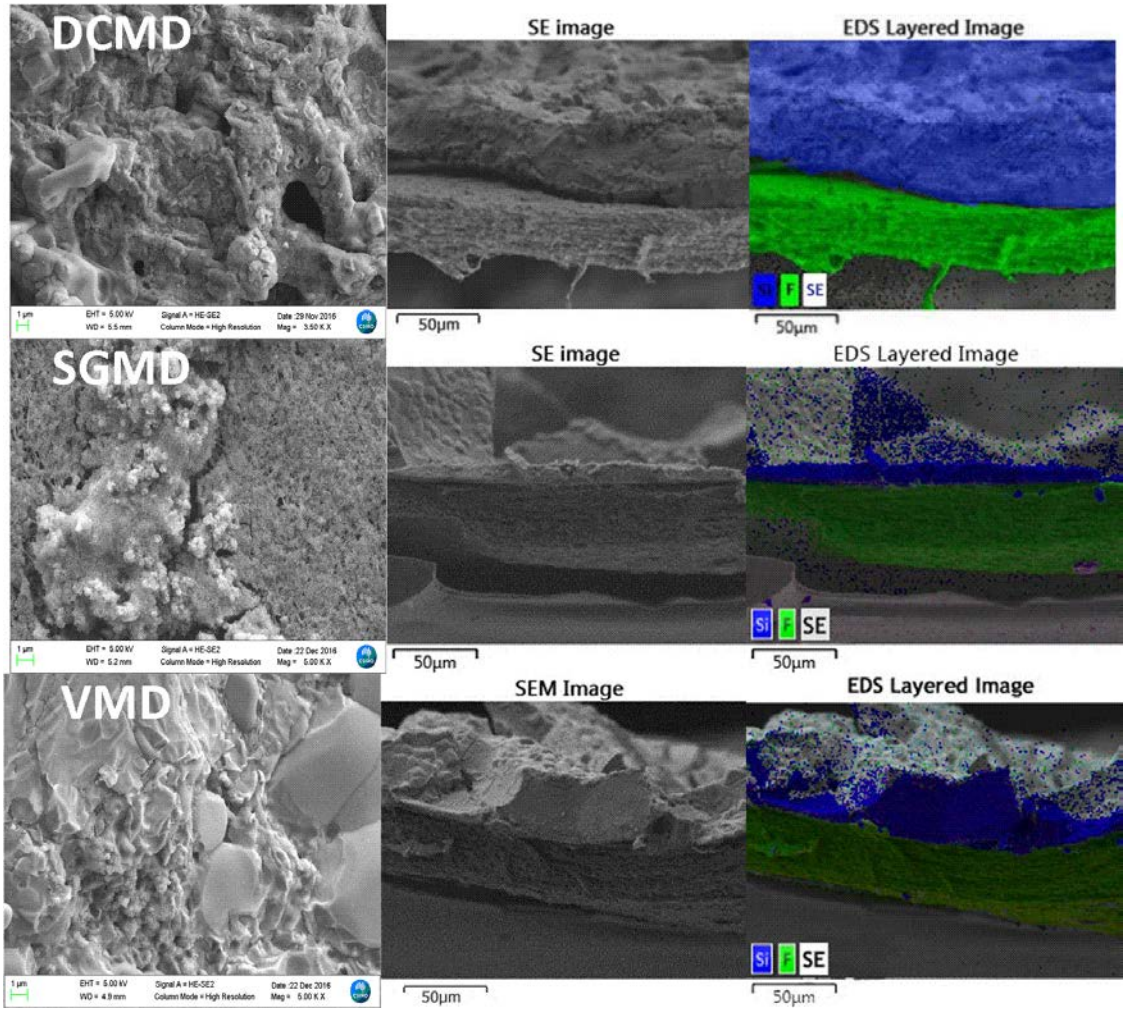
DCMD
SE image
EDS Layered Image
50µm
50µm
Si F SE
SGMD
SE image
EDS Layered Image
50µm
50µm
Si F SE
VMD
SEM Image
EDS Layered Image
50µm
50µm
Si F SE

(a) Si

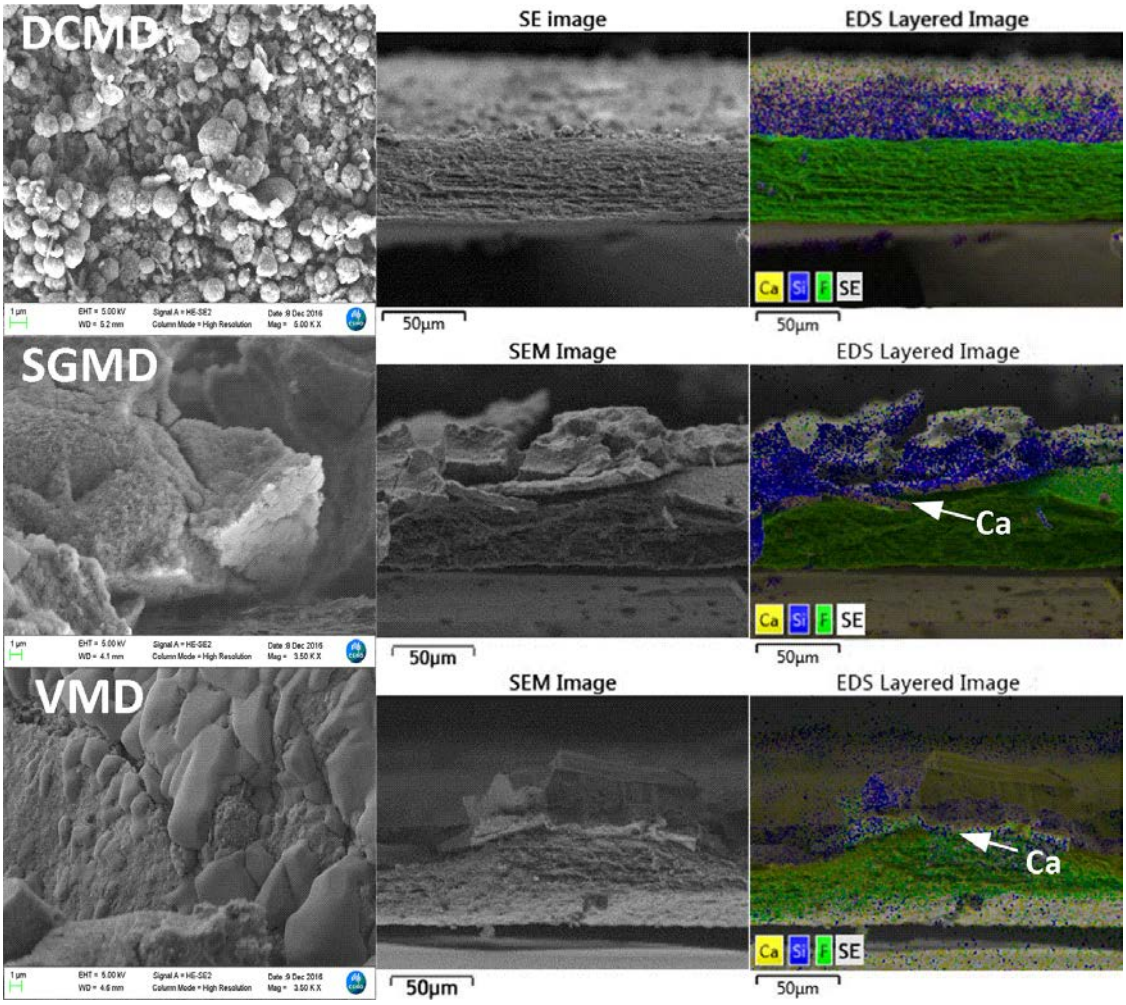
DCMD
SE image
EDS Layered Image
Ca Si F SE
50µm
50µm
SGMD
SEM Image
EDS Layered Image
Ca
Ca Si F SE
50µm
50µm
VMD
SEM Image
EDS Layered Image
Ca
Ca Si F SE
50µm
50µm

(b) Si+Ca

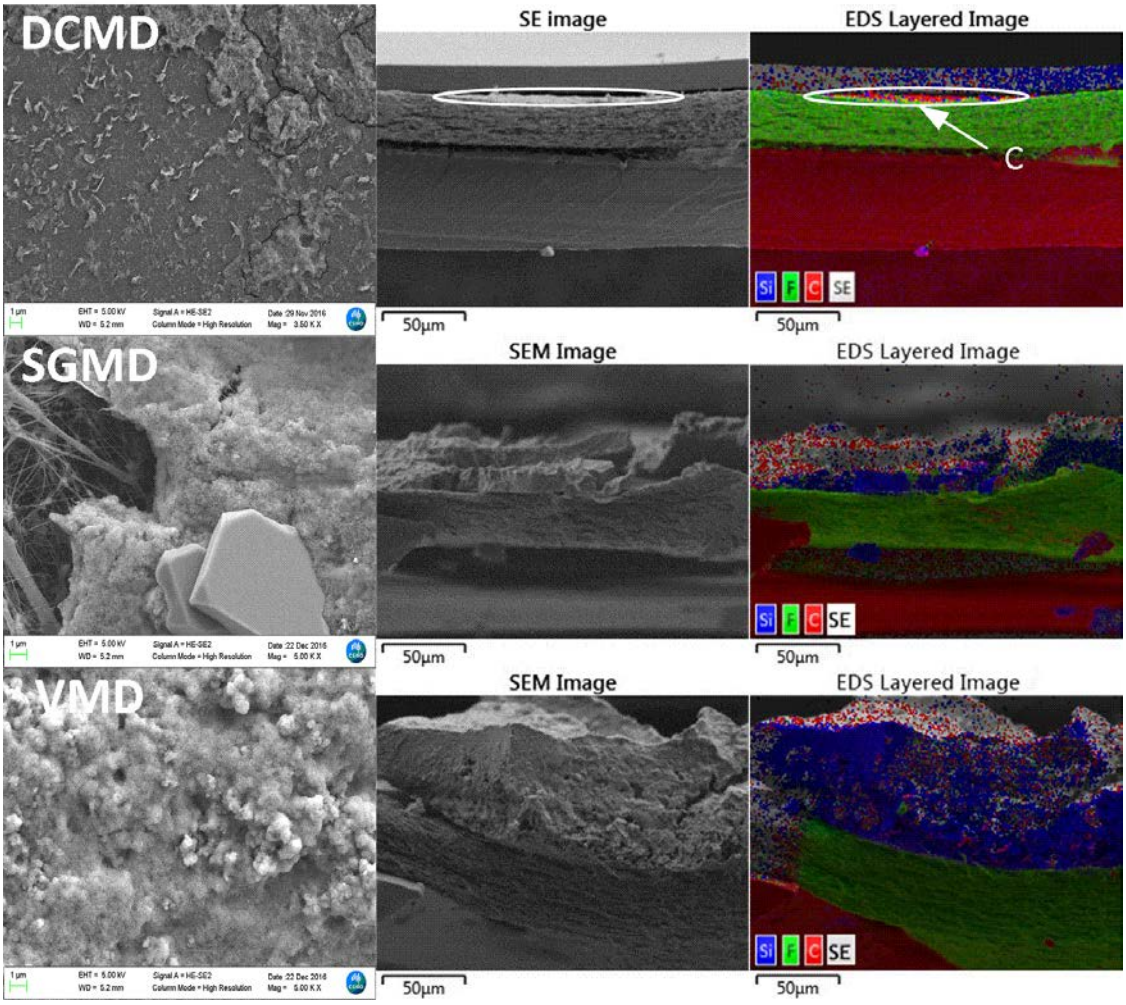
DCMD
SE image
EDS Layered Image
C
Si F C SE
50µm
50µm
SGMD
SEM Image
EDS Layered Image
Si F C SE
50µm
50µm
VMD
SEM Image
EDS Layered Image
Si F C SE
50µm
50µm

(c) Si+NOM

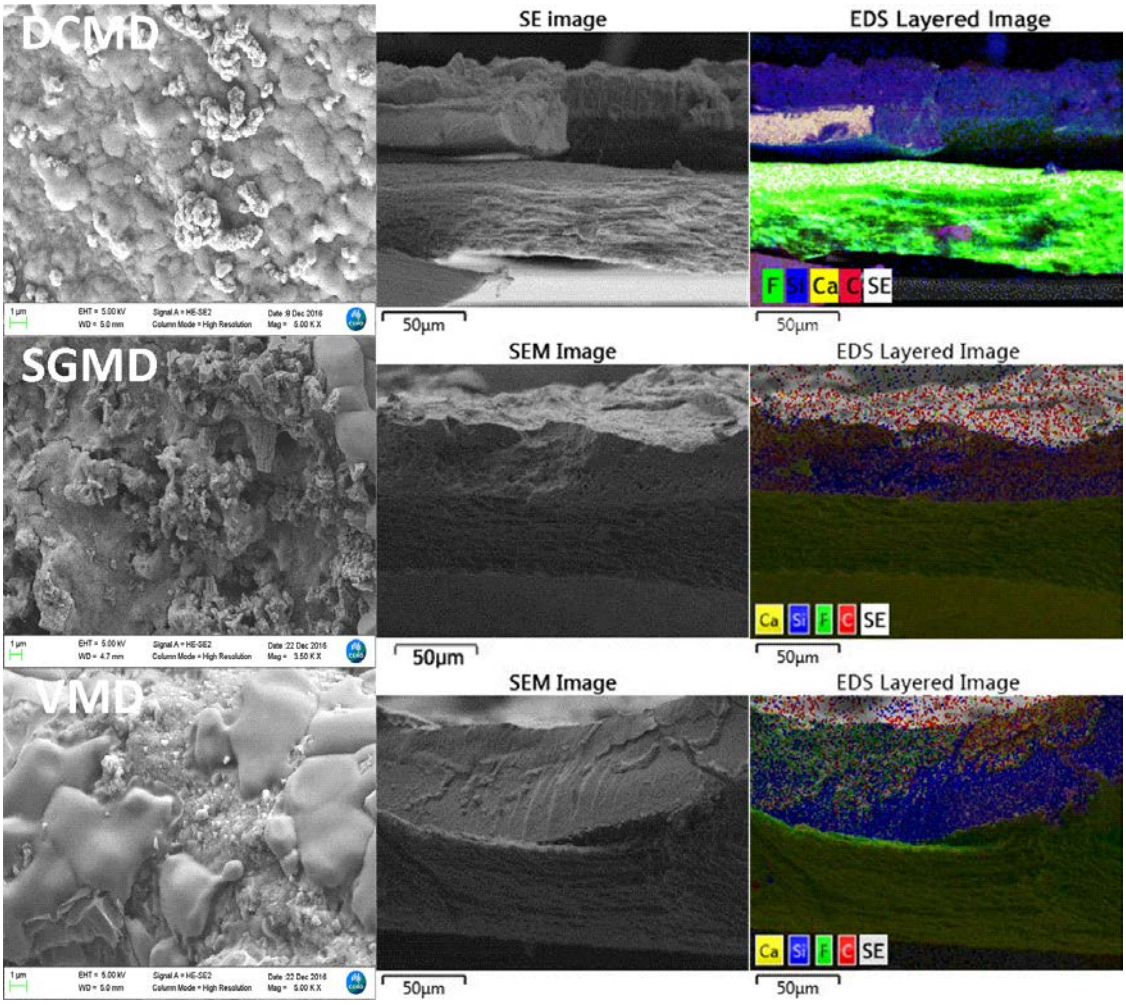

(d) Si+NOM+Ca

Figure 5. SEM and EDS he fouled membrane in different configuration: (a) Si, (b) Si+Ca, (c) Si+NOM, (d) Si+NOM+Ca

The SEM images for the feed containing the Si+Ca+NOM are shown in Figure 5(d). Calcium carbonate scaling formed on top of the fouling layer for DCMD (Figure 5(d)) and the extent of deposited material appeared less than that of the Si+Ca feed, which also corresponded to the flux decline that occurred at 24% recovery shown for the DCMD curve in Figure 2(d). Furthermore, no crystal structure was observed for the fouling layer surfaces in all configurations in Figure 5(d), and the boundary for different

foulants could not be easily identified compared to other foulant combinations, which demonstrates the existence of interaction among the those foulants.

To understand the fouling behavior further, computational fluid dynamics (CFD) and modelling of MD systems may be a useful addition to understanding the impact of MD configuration on fouling performance. Furthermore, the XPS or other surface characterization methods to autopsy the used MD membranes may also provide greater insight as to the processes occurring.

4. Conclusion

Four different combinations of three foulants including Si, Si+Ca, Si+NOM and Si+NOM+Ca were used in the study. The fouling behavior in DCMD, SGMD and VMD were compared for up to 25% feed recovery.

Although DCMD showed the highest flux in all configurations, except for Si+NOM+Ca combination. The combinations and interaction of the three foulants showed higher dependence on membrane flux incurred concentration polarization than turbulence and led to the worst fouling for DCMD process.

SGMD showed the best fouling resistance in all configurations because of its lower flux and good hydrodynamic mixing of the feed side, although it was inclined to calcium carbonate fouling due to the stripping of CO_2 from feed. However, this issue can be alleviated by using air rather than pure nitrogen as the sweeping gas, since the partial pressure of CO_2 in the air is not zero and will reduce the CO_2 depletion rate.

VMD almost showed the worst fouling resistance to most tested foulant

combinations due to the deformation of PTFE membrane under unbalanced pressure. Wetting was also incurred in VMD by the combination of fouling and relative high hydraulic pressure difference across the membrane. Therefore, the use of compressible membrane in VMD process might increase particulate fouling. Furthermore, even if an incompressible membrane was used, employing VMD in high-concentration calcium bicarbonate or carbonate foulants still needs to be avoided when there is no scale inhibitors

Based on the experimental conditions and results, it was found that the particulate fouling could be reduced by avoiding dead zones (static zone) in the flow channel. To alleviate NOM fouling, choosing an adequate flux to reduce the concentration polarization will be more effective.

5. Acknowledgement

The authors would like to acknowledge the CSIRO Manufacturing for the financial support of this work. W. Qin would like to thank the PhD student exchange scholarship from Zhejiang University. Mr Mark Greaves from CSIRO Manufacturing is greatly acknowledged for his help in SEM.

Reference:

412 Alklaibi, A.M. and Lior, N. (2005) Membrane-distillation desalination: Status and potential. Desalination
413 171(2), 111-131.
414 Bacchin, P., Aimar, P. and Field, R.W. (2006) Critical and sustainable fluxes: Theory, experiments and
415 applications. Journal of Membrane Science 281(1–2), 42-69.
416 Ballantyne, A.P., Alden, C.B., Miller, J.B., Tans, P.P. and White, J.W.C. (2012) Increase in observed net
417 carbon dioxide uptake by land and oceans during the past 50 years. Nature 488(7409), 70-72.
418 Banat, F., Jumah, R. and Garaibeh, M. (2002) Exploitation of solar energy collected by solar stills for
419 desalination by membrane distillation. Renewable Energy 25(2), 293-305.
420 Chen, V., Fane, A.G., Madaeni, S. and Wenten, I.G. (1997) Particle deposition during membrane filtration
421 of colloids: transition between concentration polarization and cake formation. Journal of Membrane
422 Science 125(1), 109-122.
423 Enríquez, O.R., Hummelink, C., Bruggert, G.-W., Lohse, D., Prosperetti, A., van der Meer, D. and Sun,
424 C. (2013) Growing bubbles in a slightly supersaturated liquid solution. Review of scientific instruments
425 84(6), 065111.
426 Frear, G. and Johnston, J. (1929) THE SOLUBILITY OF CALCIUM CARBONATE (CALCITE) IN
427 CERTAIN AQUEOUS SOLUTIONS AT 25° 1. Journal of the American Chemical Society 51(7), 2082-
428 2093.
429 Gajevskiy, V. (2015) Electric conductivity of carbon dioxide aqueous solutions. Ukrainian journal of
430 physics (60,№ 3), 258-262.
431 Geankoplis, C.J. (2003) Transport processes and separation process principles Prentice Hall Press, Saddle
432 River.
433 Gryta, M. (2008) Fouling in direct contact membrane distillation process. Journal of Membrane Science
434 325(1), 383-394.
435 Kitano, Y., Kanamori, N. and Tokuyama, A. (1969) Effects of organic matter on solubilities and crystal
436 form of carbonates. American Zoologist 9(3), 681-688.
437 Laqbaqbi, M., Sanmartino, J., Khayet, M., García-Payo, C. and Chaouch, M. (2017) Fouling in
438 Membrane Distillation, Osmotic Distillation and Osmotic Membrane Distillation. Applied Sciences 7(4),
439 334.
440 Lawson, K.W., Hall, M.S. and Lloyd, D.R. (1995) Compaction of microporous membranes used in
441 membrane distillation. I. Effect on gas permeability. Journal of Membrane Science 101(1-2), 99-108.
442 Lawson, K.W. and Lloyd, D.R. (1997) Membrane distillation. Journal of Membrane Science 124(1), 1-
443 25.
444 Lee, N., Amy, G., Croué, J.-P. and Buisson, H. (2004) Identification and understanding of fouling in low-
445 pressure membrane (MF/UF) filtration by natural organic matter (NOM). Water Research 38(20), 4511-
446 4523.
447 Lei, Z., Chen, B. and Ding, Z. (2005) Special Distillation Processes. Lei, Z., Chen, B. and Ding, Z. (eds),
448 pp. 241-319, Elsevier Science, Amsterdam.
449 Light, T.S., Kingman, B. and Bevilacqua, A.C. (1995) The Conductivity of Low Concentrations of CO2
450 Dissolved in Ultrapure Water from 0-100 C, pp. 2-6.
451 Mulder, M. (1996) Basic Principles of Membrane Technology, Kluwer, Dordrecht.
452 Phattaranawik, J., Jiraratananon, R., Fane, A.G. and Halim, C. (2001) Mass flux enhancement using
453 spacer filled channels in direct contact membrane distillation. Journal of Membrane Science 187(1-2),
454 193-201.
455 Qin, W., Zhang, J., Xie, Z., Ng, D., Ye, Y., Gray, S.R. and Xie, M. (2017) Synergistic effect of combined

colloidal and organic fouling in membrane distillation: Measurements and mechanisms. Environmental Science: Water Research & Technology 3(1), 119-127.
Rae, P.J. and Brown, E.N. (2005) The properties of poly(tetrafluoroethylene) (PTFE) in tension. Polymer 46(19), 8128-8140.
Rae, P.J. and Dattelbaum, D.M. (2004) The properties of poly(tetrafluoroethylene) (PTFE) in compression. Polymer 45(22), 7615-7625.
Schneider, K. and van Gassel, T.J. (1984) Membrandestillation. Chemie Ingenieur Technik 56(7), 514-521.
Trushina, D.B., Sulyanov, S.N., Bukreeva, T.V. and Kovalchuk, M.V. (2015) Size control and structure features of spherical calcium carbonate particles. Crystallography Reports 60(4), 570-577.
Wang, Z., Elimelech, M. and Lin, S. (2016a) Environmental applications of interfacial materials with special wettability. Environmental Science & Technology 50(5), 2132-2150.
Wang, Z., Hou, D. and Lin, S. (2016b) Composite membrane with underwater-oleophobic surface for anti-oil-fouling membrane distillation. Environmental Science & Technology 50(7), 3866-3874.
Warsinger, D.M., Swaminathan, J., Guillen-Burrieza, E. and Arafat, H.A. (2015) Scaling and fouling in membrane distillation for desalination applications: A review. Desalination 356, 294-313.
Weyl, P.K. (1967) Recovery of demineralized water from saline waters, U. S. A.
Yu, J., Lei, M. and Cheng, B. (2004) Facile preparation of monodispersed calcium carbonate spherical particles via a simple precipitation reaction. Materials Chemistry and Physics 88(1), 1-4.
Zhang, J., Dow, N., Duke, M., Ostarcevic, E., Li, J.-D. and Gray, S. (2010a) Identification of material and physical features of membrane distillation membranes for high performance desalination. Journal of Membrane Science 349(1-2), 295-303.
Zhang, J., Duke, M., Hoang, M., Xie, Z., Groth, A., Tun, C. and Gray, S. (2013a) Influence of module design and membrane compressibility on VMD performance. Journal of Membrane Science 442, 31-38.
Zhang, J., Gray, S. and Li, J.-D. (2012) Modelling heat and mass transfers in DCMD using compressible membranes. Journal of Membrane Science 387–388(0), 7-16.
Zhang, J., Li, J.-D., Duke, M., Hoang, M., Xie, Z., Groth, A., Tun, C. and Gray, S. (2013b) Modelling of vacuum membrane distillation. Journal of Membrane Science 434, 1-9.
Zhang, J., Li, J.-D., Duke, M., Xie, Z. and Gray, S. (2010b) Performance of asymmetric hollow fibre membranes in membrane distillation under various configurations and vacuum enhancement. Journal of Membrane Science 362(1), 517-528.
Zhang, J., Li, J.-D. and Gray, S. (2011) Effect of applied pressure on performance of PTFE membrane in DCMD. Journal of Membrane Science 369(1), 514-525.